Title

Incorporation of Ni2+, Co2+, and Selenocysteine into the Auxiliary Fe-S Cluster of the Radical SAM Enzyme HydG

Journal

Inorganic Chemistry, 58(19)

ISSN

0020-1669

Authors

Rao, Guodong
Alwan, Katherine B
Blackburn, Ninian J
et al.

Publication Date

2019-10-07

DOI

10.1021/acs.inorgchem.9b01293

Peer reviewed

HHS Public Access

Author manuscript

Inorg Chem. Author manuscript; available in PMC 2020 October 07.

Published in final edited form as:

Inorg Chem. 2019 October 07; 58(19): 12601–12608. doi:10.1021/acs.inorgchem.9b01293.

Incorporation of Ni^{2+}, Co^{2+} and selenocysteine into the auxiliary Fe-S cluster of the radical SAM enzyme HydG

Guodong Rao[†], **Katherine B. Alwan**[‡], **Ninian J. Blackburn**[‡], **R. David Britt**[†]

[†]Department of Chemistry, University of California, Davis, CA 95616, USA

[‡]Department of Chemical Physiology and Biochemistry, Oregon Health and Science University, Portland, OR 97239, USA

Abstract

The radical SAM enzyme HydG generates CO and CN^- -containing Fe complexes that are involved in the bioassembly of the [FeFe] hydrogenase active cofactor, the H-cluster. HydG contains a unique 5Fe-4S cluster in which the fifth "dangler" Fe and the coordinating cysteine molecule have both been shown to be essential for its function. Here, we demonstrate that this dangler Fe can be replaced with Ni^{2+} or Co^{2+}, and that the cysteine can be replaced with selenocysteine. The resulting HydG variants were characterized by electron paramagnetic resonance and X-ray absorption spectroscopy, as well as subjected to a Tyr cleavage assay. Both Ni^{2+} and Co^{2+} are shown to be exchange-coupled to the 4Fe-4S cluster, and selenocysteine substitution does not alter the electronic structure significantly. XAS data provides details of the coordination environments near the Ni, Co, and Se atoms, and supports a close interaction of the dangler metal with the FeS cluster via an asymmetric SeCys bridge. Lastly, while we were unable to observe formation of novel organometallic species for the Ni^{2+} and Co^{2+} variants, the selenocysteine variant retains the activity of wildtype HydG in forming $[Fe(CO)_x(CN)_y]$ species. Our results provide more insights into the unique auxiliary cluster in HydG and expand the scope of artificially generated Fe-S clusters with heteroatoms.

Graphical Abstract

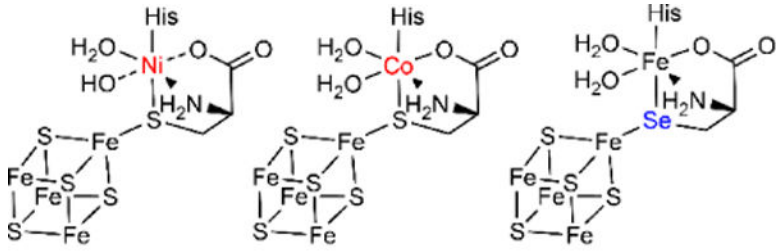

blackbni@ohsu.edu, rdbritt@ucdavis.edu.

ASSOCIATED CONTENT

Supporting information (nine Figures and one Table) containing EPR spectra and alternative fits of Se, Co and Ni EXAFS spectra.

The authors declare no competing financial interest.

INTRODUCTION

Biological iron-sulfur clusters are widespread metallocofactors that play significant roles in maintaining structural integrity, mediating electron transfer, and performing redox and non-redox catalysis.[1–8] While canonical Fe-S clusters consist of only Fe and S atoms categorized according to their Fe:S stoichiometry, Fe-S clusters containing heteroatoms are also found in enzymes that catalyze fascinating reactions. For examples, Mo/V-Fe-S clusters in nitrogenases are essential for reducing N_2 to ammonia,[7] while Ni-Fe-S clusters in carbon monoxide dehydrogenase/acetyl-CoA synthase (CODH/ACS) are essential for reducing CO_2 and fixing CO (Scheme 1A).[8] Incorporation of heteroatoms into biological Fe-S clusters is therefore of interest to better understand their properties as well as to uncover new functions.

The most frequently used synthetic method to site-specifically incorporate a heteroatom into a Fe-S cluster is accomplished by removing the non-cysteinyl-coordinated Fe from a 4Fe-4S cubane, e.g. that in *Pyrococcus furiosus* ferredoxin which is coordinated by three cysteine (Cys) and one aspartate residue, followed by placing a different metal ion into the vacant apical site (Scheme 1B). A series of MFe_3S_4 (M = Co, Ni, Zn, Cd, Cu, Cr…) clusters that share structural features of the FeMoCo cofactor have been generated in this manner,[9–13] each exhibiting unique spectroscopic features and redox properties. While this approach has proven to be fruitful, the geometric scope of the resulting cluster is rather limited. Expanding our capability to generate different heteroatom clusters is desirable to emulate the naturally existing Fe-S clusters with varying compositions and geometries.

The radical SAM enzyme HydG, involved in the bioassembly of the [FeFe] hydrogenase H-cluster, is an interesting platform for this purpose. HydG harbors a unique 5Fe-4S auxiliary cluster, recently identified from X-ray crystallographic analysis with support from biochemical and spectroscopic studies.[14–16] In this 5Fe-4S cluster, a high-spin “dangler” Fe^{2+} ($S = 2$) is chelated by a Cys molecule through which it is linked to a conventional $[4Fe\text{-}4S]^{+}$ cluster ($S = 1/2$) via an bridging S atom, forming an $S = 5/2$ resting state (Scheme 2A). We have previously shown that this Fe^{2+} can be removed by EDTA, leaving behind a 4Fe-4S cluster coordinated by three proteinaceous Cys residues and an apical Cys molecule.[14] Interestingly, the Cys molecule in this [4Fe-4S][Cys] cluster can be exchanged by Cys analogues (e.g. isotopologues), and the 5Fe-4S cluster can be restored by adding back the Fe^{2+} ion (Scheme 2B).[14, 17] The lability of the dangler Fe and the bridging Cys has allowed us to site-specifically label HydG for mechanistic studies revealing the role of the auxiliary cluster as a platform for generating the $[Fe(CO)_2(CN)(Cys)]^{-}$ organometallic precursor in H-cluster bioassembly.[17] Meanwhile, we envision that it also provides an opportunity to install heteroatoms into the auxiliary cluster to afford artificial Fe-S clusters that share structural features with ACS and may exhibit novel functions.

In this paper, we report the incorporation of Ni, Co or Se atoms into the auxiliary cluster of HydG. The resulting HydG variants are characterized by electron paramagnetic resonance (EPR) and X-ray absorption spectroscopy (XAS), as well as subjected to enzymatic assays. These results provide more insights into the coordination environments of the auxiliary Fe-S cluster in HydG and expand our scope of artificially generated biological Fe-S sites.

MATERIALS AND METHODS

General considerations.

All chemicals were purchased from Sigma-Aldrich (Milwaukee, WI) unless specified. Purification of HydG and preparation of EPR and XAS samples were performed in an anaerobic chamber with O_2 level < 2 ppm.

Protein Purification.

Shewanella oneidensis HydG and the radical SAM cluster-knockout mutant ($HydG^{\Delta RS}$) were expressed in a recombinant *E. coli* BL21(DE3) *ΔiscR* strain and purified by Strep-tag affinity chromatography as described previously.[17]

Sample preparation.

The dangler Fe in the HydG auxiliary cluster was removed by adding EDTA followed by buffer exchange as described previously.[14, 17] Briefly, to 300 μM of HydG or $HydG^{\Delta RS}$ was added 600 μM EDTA and 3 mM each of dithionite, SAM (SAM is not required with $HydG^{\Delta RS}$, see below), and cysteine. The mixture was incubated at room temperature for 10 min, diluted by 10-fold using a buffer containing 3 mM each of dithionite, SAM and Cys, and then concentrated into the original volume using a 30 kDa cutoff Amicon Ultra centrifugal filter. The HydG-Ni and HydG-Co samples were made by adding 1 mM of Ni^{2+} or Co^{2+} into the resulting solution, respectively. For XAS samples, the buffer exchange steps were repeated three times against a solution containing 3 mM dithionite and 3 mM Cys to remove the excess metal ions. To make the HydG-SeCys sample, to 300 μM of HydG was added 6 mM dithionite, 3 mM SAM, 3 mM selenocystine and 600 μM EDTA. The resulting mixture was diluted by 10-fold using a buffer containing 6 mM dithionite, 3 mM SAM and 3 mM selenocystine and concentrated back to the original volume. This step was repeated twice to remove the residual Cys. HydG-SeCys was then generated by added 1 mM Fe^{2+} to the resulting solution. For XAS samples, the excess SeCys was removed by three cycles of buffer exchange against a solution containing 3 mM dithionite.

To make HydG variants for enzyme activity assays, Co, Ni or SeCys were incorporated into native HydG (with both RS and auxiliary clusters present) as described above. Procedures for generating EPR samples containing the 4-OB radical and Complex A were as previously described.[17–18]

EPR spectroscopy.

EPR spectroscopy was performed at the CalEPR center at the University of California, Davis. Continuous wave (CW) EPR spectra were collected on a Bruker Biospin EleXsys E500 spectrometer equipped with a super high Q resonator (ER4122SHQE). Cryogenic temperature was achieved by using an ESR900 liquid helium cryostat with a temperature controller (Oxford Instrument ITC503) and a gas flow controller. CW EPR spectra were recorded under slow-passage, non-saturating conditions with the following spectrometer settings: conversion time = 60 ms (sweep time = 60 s for 1000 data points), modulation amplitude = 0.5 mT, modulation frequency = 100 kHz. Other experimental parameters are

given in the corresponding figure captions. Simulations of EPR spectra were performed in Matlab R2018a with the EasySpin 5.2.15 toolbox.[19]

Collection and Analysis of XAS Data.

Samples were measured as aqueous glasses in 20 percent ethylene glycol at 10 K. Co (7709 eV), Ni (8333 eV), and Se (12658 eV) extended X-ray absorption fine structure (EXAFS) and X-ray absorption near edge structure (XANES) data were collected on beam line 9.3 at the Stanford Synchrotron Radiation Lightsource operating at 3 GeV with currents close to 500 mA maintained by continuous top-off. All data collection used a Si[220] monochromator and a Rh-coated mirror upstream (set at 10 keV energy cutoff for Co, 12 keV energy cut-off for Ni, and 15 keV energy cutoff for Se) in order to reject harmonics. Data were collected in fluorescence mode using a high-count rate Canberra 100-element Ge array detector with maximum count rates per array element less than 120 kHz. A 'Z-1' metal (Se) or metal oxide (Co, Ni) filter and Soller slit assembly inserted in front of the detector was used to reduce elastic scattering relative to the absorber Kα fluorescence. Energy calibration was achieved by simultaneous measurement of a metal calibration foil placed between the second and third ionization chambers. The first inflexion points of the metal spectra were used to calibrate the monochromator to 7709.0 eV for Co, 8331.6 eV for Ni and 12658.0 for Se. Four to six scans of a sample containing only buffer were averaged and subtracted from the averaged data for each protein sample to remove the Z-1 Kβ fluorescence from the filter, and produce a flat pre-edge baseline.

Data reduction and background subtractions were performed using the program modules of EXAFSPAK [20]. Output from each detector channel was inspected for glitches and dropouts before inclusion in the final average. Spectral simulation was carried out using EXCURVE version 9.2 [21] as described previously [22–23]. Simulations of the EXAFS data used a mixed-shell model consisting of imidazole from histidine residues, O/N scatterers from non-His ligands, S from cysteine coordination (or Se from selenocysteine), and Fe and/or S scatterers from nearby Fe-S clusters. The threshold energy, E_0, was chosen at 7714 eV for Co, 8338 eV for Ni and 12663 eV for Se. Parameters floated in the fits included distances (R), coordination numbers (N, integer values only), and Debye-Waller factors (σ^2), and included multiple scattering contributions from outer-shell atoms of imidazole rings.

RESULTS AND DISCUSSION

Incorporation of Ni^{2+} and Co^{2+} into the auxiliary cluster.

In order to test what metal ions can be incorporated into the auxiliary cluster of HydG, we used a HydG mutant that lacks the N-terminal radical SAM ($HydG^{\Delta RS}$) cluster to minimize the interference of the RS cluster, and prepared the dangler Fe-removed protein as described.[14, 17] A series of metal ions were added to the resulting [4Fe-4S][Cys] cluster and the EPR spectra were recorded before and after metal ion addition (Figure S1). The dithionite-reduced [4Fe-4S][Cys] cluster exhibits a near axial $S = 1/2$ EPR signal with $g = [2.063, 1.908, 1.876]$ (Figure 1A), which can be converted into the $S = 5/2$ [4Fe-4S][Fe(Cys)] auxiliary cluster by adding Fe^{2+} (Figure 1B). The [4Fe-4S][Cys] signal disappears after incubating with Ni^{2+} (d^8, $S = 1$), accompanied by the formation of EPR features with

effective g-values of 4.8 and 3.6 as previously observed (Figure 1C),[14] indicating that Ni^{2+} is incorporated into the dangler position, and is exchange coupled to the $[4Fe\text{-}4S]^{+}$ cluster, forming [4Fe-4S][Ni(Cys)] species with a total spin of $S = 3/2$. Formation of the $S = 3/2$ signals is an indication that Ni has replaced the dangler Fe site. EPR spectra recorded at different temperatures indicate that the relative intensity between these two EPR features doesn't change at different temperatures (Figure S2), suggesting that they originate from the same $m_s = \pm 1/2$ Kramer doublet according to the rhombogram of $S = 3/2$ spin system (Figure S3). Interestingly, EPR features with g_{eff} of 4.8 and 3.6 do not correspond to the same E/D, implying that they probably represent different species in somewhat different coordination environments which arise from heterogeneity in the local environment of the auxiliary cluster. Due to the absence of any recognizable feature corresponding to $m_s = \pm 3/2$ doublets (which would appear at $5.46 < g_{eff} < 6$), the zero field splitting parameters, E and D, are not measured. Nevertheless, lack of these features implies a positive $D >> kT$.

The [4Fe-4S][Cys] signal also disappears after the addition of Co^{2+} (Figure 1D), suggesting that Co^{2+} may also be incorporated into the dangler position. Further addition of EDTA followed by buffer exchange restores the [4Fe-4S][Cys] signal, suggesting that the 4Fe-4S cluster is intact in the presence of Co^{2+} (Figure 1D). The disappearance of the EPR signal is therefore best explained by exchange coupling between the $S = 1/2$ Fe-S cluster and the S = 3/2 high spin Co^{2+}, leading to the proposed [4Fe-4S][Co(Cys)] species that could be either $S = 2$ or 1, resulting from ferromagnetic or antiferromagnetic coupling between Co^{2+} and the [4Fe-4S] cluster respectively. No EPR signals corresponding to these integer spin systems were observed, and therefore we further characterized the Co complex by XAS experiments (vide infra).

Lastly, while the [4Fe-4S][Cys] signal is also reduced after the addition of Cu^{2+} (Figure S1), formation of CuS (or Cu_2S) precipitates was also observed, indicating that the Fe-S cluster may have been damaged, releasing Fe^{2+} from the 4Fe-4S cluster and leading to the formation of a small amount of [5Fe-4S] cluster. No high spin species were observed as reported for a [Cu-3Fe-4S] cluster.[13] Addition of other metal ions did not change the EPR spectra significantly (Figure S1).

Incorporation of selenocysteine into the auxiliary cluster.

The [4Fe-4S][Cys] cluster was buffer-exchanged against a selenocysteine (SeCys)-containing solution to the furnish the [4Fe-4S][SeCys] cluster. The EPR spectrum of the resulting species is slightly different from the Cys analogue, with g-values = [2.059, 1.895, 1.859] (Figure 1E). The corresponding g_{iso} of 1.940 ($g_{iso}^2 = 1/3 \times (g_1^2 + g_2^2 + g_3^2)$) has slightly larger deviation from g_e than the g_{iso} of 1.950 for the [4Fe-4S][Cys] species, likely caused by a larger spin-orbital coupling of Se compared to S. Due to the low abundance of the magnetic ^{77}Se ($I = 1/2$, 7.6%), use of pulsed EPR experiments in attempt to probe the hyperfine coupling to Se has not been fruitful, and the interaction between Se and the Fe-S cluster was investigated by XAS (*vide infra*). Addition of Fe^{2+} to the [4Fe-4S][SeCys] cluster leads to the formation of an $S = 5/2$ species that exhibits EPR features with effective g-values of 9.4, 4.6, and 3.9 (Figure 1F), similar to the [4Fe-4S][Fe(Cys)] analogue,[14] indicating that the electronic structure of the auxiliary cluster is not dramatically affected by

the presence of the Se atom. Referring to the rhombogram of the $S = 5/2$ spin system (Figure S4), the $g_{eff} = 9.4$ and $g_{eff} = 4.6$, 3.9 features originate from the EPR transitions within the $m_s = \pm 1/2$ and the $m_s = \pm 3/2$ Kramer doublet respectively, and they correspond to an E/D value of ~0.25 that is similar to the value found in the Cys analogue. The relative intensity between the $g_{eff} = 9.4$ and $g_{eff} = 3.9$ features at different temperatures reflects the relative population of the $m_s = \pm 1/2$ and $m_s = \pm 3/2$ states governed by Boltzmann distribution. Accordingly, the zero field splitting parameter D was measured to be +3.5 cm^{-1} (Figure S5). This D value is somewhat different from the +4.5 cm^{-1} found in the Cys analogue.[14] In short, our EPR spectroscopic results demonstrated that we were able to incorporate Ni, Co and Se atoms into the auxiliary Fe-S cluster in HydG, and their interactions with the Fe-S clusters are further probed by XAS studies.

X-ray absorption spectroscopy.

One of the advantages of substituting the dangler Fe by other metals is that it allows the dangler atom to be visualized independent of the other Fe atoms that constitute the Fe-S clusters in HydG. In native HydG, the coordination of the dangler Fe atom has been suggested to be connected to the FeS cluster via the apical Cys molecule which bridges between a Fe atom of the cluster and the dangler Fe atom through Cys S atom. This proposal is supported by X-ray crystallography studies, as well as the $S = 5/2$ spin state of the 5Fe cluster, as shown in scheme 2.[14, 16] When the dangler Fe atom is substituted by Ni or Co, the exchange interaction between the heteroatoms and the FeS cluster observed by EPR spectroscopy implies that they are in close proximity to the FeS, yet other modes of coordination are still possible. Since the cysteine can be substituted by selenocysteine, the XAS data on the SeCys derivative of the native Fe protein can be used to probe the dangler Fe atom from the perspective of the Se edge since data from the Fe edge is overwhelmed by contributions from the Fe-S cluster. Different modes of coordination of the exogenous cysteine lead to three different unique predictions for the Se-Fe scattering in the EXAFS each of which has been probed by simulation. Scenario 1 supposes symmetrical bridging of the SeCys ligand between the FeS and the dangler Fe leading to observation of 2 Se-Fe interactions; scenario 2 supposes terminal coordination of SeCys to the dangler Fe leading to 1 Se-Fe interaction; a third scenario is an asymmetrical bridge with two Se-Fe interactions with different Se-Fe distances.

The Se K Fourier transform and EXAFS are shown in Figure 2A with the Se XANES in Figure 2B. The experimental data show a low-R shoulder assignable to Se-C from SeCys together with two strong peaks at or above 2.4 Å. For symmetric bridging it is anticipated that the 2.4 Å peak would correspond to Se-Fe, while the peak at higher R would arise from additional scattering from a nearby shell such as S from the cluster. Simulations using 2 Se-Fe interactions to simulate the 2.4 Å peak and a S shell to simulate the other peak (Table S1 Se Fit #2) give a poor fit to the data with least squares residual (Fit Index, FI) of 4.6. More specifically, the Debye Waller factor for the Se-Fe shell is large ($\sigma^2 = 0.010$ $Å^2$), and three times that of the bridging SeCys ligand previously reported for SeCys labeling of Cu(I)-CCS.[24] The symmetric bridging fit (shown for comparison in Figure S6) was therefor considered unacceptable on the basis of the high FI and the unreasonable value of the DW. The second scenario corresponding to a terminal Fe-SeCys interaction was also explored and

gave a more reasonable value for the DW (0.003 $Å^2$) with a much improved FI (1.84, Table S1, Se Fit#1, Figure S7). However, terminal coordination of SeCys is not consistent with the $S = 5/2$ spin state of the dangler Fe which arises from coupling of an $S = 2$ Fe(II) center with the $S = 1/2$ spin state of the FeS cluster. Therefore, we explored the third scenario of asymmetric bridging where the 2.4 Å peak represents one Se-Fe interaction, and the higher R peak represents a second Se-Fe interaction. Simulations using this model gave fits of excellent quality, with one Se-Fe at 2.42 Å and a second Se-Fe at 2.62 Å, both with low DW factors in the expected range. This fit is shown in Figure 2A with metrical parameters listed in Table 1.

The asymmetric bridging model is most consistent with all of the data. First as discussed above, it is consistent with the $S = 5/2$ spin state of the dangler Fe, which is only observed in the presence of added cysteine. Second, it is consistent with and extends the structural model of the 5Fe-4S cluster as visualized by the crystal structure of HydG (PDB ID: 4WCX[16]). This structure shows the dangler Fe connected to a FeS cluster via an asymmetric μ-sulfido bridge with bond lengths of 2.25 and 2.52 Å for the Fe-S (cluster) and Fe-S (dangler) bonds respectively. This structure shows a free alanine amino acid rather than a cysteine coordinated to the dangler Fe, but further studies[14, 25] have determined that it most likely reflects an asymmetric bridging cysteine with the density for the C-S bond missing. This would imply that in native HydG a free cysteine bridges between an Fe atom of the cluster and the dangler Fe in the same way that we have determined for the SeCys in the present study. Given the larger radius of Se vs S, it is reasonable for us to assign the Se-Fe interaction of 2.42 Å to the Se-Fe bond between the bridging Se and the Fe-S cluster, and the Se-Fe interaction of 2.62 Å to the Se-Fe bond between bridging Se and the dangler Fe.

In addition to these first-shell features, the Se FT is unusually rich in outer shell features between 4 and 5 Å. While difficult to simulate with high confidence, inclusion of Se-Fe scatterers at with distances in the 4 – 5 Å range can model the data and improve the fit. We stress that this interpretation must be taken with caution, but we note that such features are not seen in Se EXAFS of selenomethionine terminally coordinated to Cu(I)[26] and may be unique to the HydG system. However, because of the low confidence associated with these interactions, they have been omitted from Figures 2 and S7.

Next we investigated systems where the native Fe dangler atom was substituted by Co or Ni. Figure S8 compares the Fourier transform intensity of the Co and Ni derivatives. It is evident that the Co system has a much more intense first shell peak suggestive of a higher coordination number. Figures 2C–F show absorption edges (D, F) and simulated EXAFS and FTs (C, E) for the Co and Ni systems respectively with the parameters used in the fits listed in Table 1. The Co system exhibits a weak 1s → 3d transition at 7710.1 eV with a featureless rising edge (midpoint 7720 eV) most characteristic of either Co(II) or Co(III).[27] As suggested by the increased FT intensity, the data were best fit by 6 first-shell ligands, with contributions from 1 Co-S, 1 Co-N(His), and 4 Co-N/O from non-His ligands. Fits that included 2 Co-S interaction and lower N/O shell occupancy were comparable to those with 1 Co-S (Table S1 and Figure S7) indicating that the metal EXAFS does not distinguish between bridging and terminal Cys coordination: in the latter case the dangler metal could for example be coordinated by a S atom of the FeS cluster or bridged to the cluster via a μ-

sulfido linkage. The DW factors for the first shell ligands to Co are chemically reasonable with values in the range 0.002 – 0.004 $Å^2$. Notwithstanding, there is some uncertainty regarding the first shell coordination numbers for the Co data, as the sample contains 4 Fe atoms from the FeS cluster which generate X-ray scattering that overlaps the Co absorption edge and may lead to small inaccuracies in normalization. The data also show outer-shell interactions arising from a feature best simulated by Co-Fe at 2.70 Å, consistent with close association with an Fe-S cluster.

The Ni absorption edge shows two features, a weak 1s → 3d transition centered at 8331.9 eV and a more intense 1s → 4p transition centered at 8336.4 eV. These features are typical of 4-coordinate Ni(II), and have been observed in complexes containing mixed Ni-N/Ni-S coordination. In particular, the spectrum is similar to that reported for the Ni(II) form of Ni-SOD, where the Ni is coordinated by the amino-terminus, and amide N of Cys2, and two additional thiolates from cysteine residues (C2 and C6) [28–30]. EXAFS analysis is consistent with a similar 2Ni-O/N + 2Ni-S ligand set in the Ni derivative of HydG where the exogenous cysteine could coordinate the Ni atom via its amino terminus and its thiolate side chain, with additional ligation from protein-based ligands (Table S1 and Figure S7). However, a fit with only 1 Ni-S (Figure 2E) has a slightly lower least-squares residual suggesting that an alternative structure with 2 O/N, 1 N(His) and 1 S is slightly more consistent with the data. Additionally, the Ni data does not exhibit detectable Ni-Fe scattering. These differences between Co and Ni coordination likely arise primarily from the different coordination preferences of the two metal ions, but also suggest that the Ni system may reorient such that an interaction with the Fe atom is not observed. We cannot exclude the possibility that the Ni atom is coordinated such that interaction with either the Fe-S cluster and/or the exogenous cysteine is disrupted relative to the native Fe or Co dangler metals.

Enzyme activity of the HydG variants.

Our EPR and XAS spectroscopic characterizations suggest the incorporation of Ni, Co or Se atoms in HydG. It is therefore of interest to test the enzyme activity of the resulting HydG variants. Specifically, we sought to test whether the Tyr cleavage activity and organometallic precursor formation activity are retained in these variants. To be noted, in the EPR and XAS studies mentioned above, we used the HydG mutant that lacks the N-terminal radical SAM Fe-S cluster ($HydG^{\Delta RS}$) to minimize the interference of the RS cluster. Here, in order to examine the enzyme activity, we used the wildtype HydG that has both RS and the auxiliary cluster. The presence of the RS cluster does not affect the incorporation of heteroatoms into HydG, as shown in the corresponding EPR spectra of HydG variants (Figure S9). For the Ni^{2+} and Co^{2+} incorporated HydG, we were able to detect the formation of the 4-hydrozylbenzyl radical when the HydG reaction is quenched at 30 s (Figure 3A), which is characteristic for the Tyr cleavage activity rendered by the RS cluster.[18] This is not surprising since the RS cluster is kept intact during the incorporation of these atoms. However, detection of organometallic species containing CO and CN^- ligands, i.e. the [4Fe-4S][(Cys)Ni(CO)(CN)] and [4Fe-4S][(Cys)Co(CO)(CN)] species, is not yet fruitful. For the SeCys incorporated HydG, the EPR spectrum of the reaction mixture containing 1 eq. Tyr and excess SAM and dithionite freeze-quenched at 30 s exhibits complex features

similar to that found in the 24 s reaction of native HydG (Figure 3B).[17] Similar to the scenario in native HydG, simulation of the spectrum also reveals three $S = 1/2$ EPR species: the SAM bound radical SAM cluster with $g = [2.0094, 1.880, 1.842]$ (blue trace), an unknown species with $g = [2.033, 1.936, 1.900]$, and lastly the [4Fe-4S][Fe(CO)(CN)(SeCys)] intermediate, i.e. the "Complex A" with Cys replaced by SeCys with $g = [2.062, 1.905, 1.880]$. The g tensor for the SeCys-Complex A is similar but different from the Cys analogue ($g = [2.058, 1.922, 1.881]$), which also supports the premise that SeCys is indeed placed in the cluster. These observations strongly suggest that the SeCys incorporated HydG can generate a modified organometallic product, which, in combination with other Fe-S enzymes in the H-cluster maturation machinery, has the potential to site-specifically incorporate Se atoms into the H-cluster via the *in vitro* "cell-free" synthesis approach.[31–32]

CONCLUSION

In summary, our biochemical and spectroscopic results have demonstrated that Ni^{2+}, Co^{2+} and SeCys can be incorporated into the auxiliary Fe-S cluster HydG to furnish artificial Fe-S clusters with site-specific modifications. These HydG variants were characterized by EPR and XAS spectroscopy, as well as subjected to enzymatic assays. These results are of interest for several aspects. First, we have shown that HydG is a versatile platform that may allow additional modification to be carried out. For instance, the promiscuity of the Cys ligand may be further examined, and the effects of this ligand on the activity of HydG, as well as H-cluster maturation may be explored. This approach benefits from the catalytic nature of HydG as forming a labile organometallic precursor, which further highlights the uniqueness of this radical SAM enzyme. Second, substituting the dangler metal ions by Ni^{2+} or Co^{2+} allows us to provide more insights by XAS into the coordination environment of the dangler metal ions that has only been characterized previously by EPR and Mössbauer spectroscopy. The combination of EPR and EXAFS, particularly the SeCys substitution has suggested an asymmetric bridging mode for the exogenous cysteine, together with a 6-coordinate dangler metal with O/N coordination positions that suggest solvent coordination, and hence vacant positions for binding of CO and CN. Lastly, unlikely previous artificial heterometal Fe-S clusters that are primarily generated in non-catalytic ferredoxin proteins, our efforts to construct artificial Fe-S clusters in an enzyme could have the potential to uncover new chemistry catalyzed by these cofactors. Starting from the SeCys-substituted HydG, it should be possible to generate the Se-atom substituted H-cluster, the biochemical and spectroscopic investigation of which could provide more insights into the activity and mechanism of H-cluster catalysis.

Supplementary Material

Refer to Web version on PubMed Central for supplementary material.

ACKNOWLEDGMENTS

This work was funded by National Institute of Health (1R35GM126961 to RDB and R01GM123725 to NJB). Use of the Stanford Synchrotron Radiation Lightsource, SLAC National Accelerator Laboratory, is supported by the U.S. Department of Energy, Office of Science, Office of Basic Energy Sciences under Contract No. DE-AC02-76SF00515. The SSRL Structural Molecular Biology Program is supported by the DOE Office of Biological

and Environmental Research, and by the National Institutes of Health, National Institute of General Medical Sciences (including P41 GM103393)

REFERENCES

1. Flint DH; Allen RM, Iron−Sulfur Proteins with Nonredox Functions. Chem. Rev 1996, 96 (7), 2315–2334. [PubMed: 11848829]
2. Beinert H; Holm RH; Munck E, Iron-sulfur clusters: nature's modular, multipurpose structures. Science 1997, 277 (5326), 653–9. [PubMed: 9235882]
3. Johnson DC; Dean DR; Smith AD; Johnson MK, Structure, function, and formation of biological iron-sulfur clusters. Annu. Rev. Biochem 2005, 74, 247–81. [PubMed: 15952888]
4. Broderick JB; Duffus BR; Duschene KS; Shepard EM, Radical S-adenosylmethionine enzymes. Chem. Rev 2014, 114 (8), 4229–4317. [PubMed: 24476342]
5. Wang W; Oldfield E, Bioorganometallic chemistry with IspG and IspH: structure, function, and inhibition of the [Fe(4)S(4)] proteins involved in isoprenoid biosynthesis. Angew. Chem. Int. Ed. Engl 2014, 53 (17), 4294–310. [PubMed: 24481599]
6. Beinert H; Kennedy MC; Stout CD, Aconitase as Iron−Sulfur Protein, enzyme, and iron-regulatory Protein. Chem. Rev 1996, 96 (7), 2335–2374. [PubMed: 11848830]
7. Burgess BK; Lowe DJ, Mechanism of molybdenum nitrogenase. Chem. Rev 1996, 96 (7), 2983–3012. [PubMed: 11848849]
8. Can M; Armstrong FA; Ragsdale SW, Structure, Function, and mechanism of the nickel metalloenzymes, CO dehydrogenase, and acetyl-CoA synthase. Chem. Rev 2014, 114 (8), 4149–4174. [PubMed: 24521136]
9. Conover RC; Park JB; Adams MWW; Johnson MK, Formation and properties of an iron-nickel sulfide (NiFe3S4) cluster in Pyrococcus furiosus ferredoxin. J. Am. Chem. Soc 1990, 112 (11), 4562–4564.
10. Moura I; Moura JJG; Munck E; Papaefthymiou V; LeGall J, Evidence for the formation of a cobalt-iron-sulfur (CoFe3S4) cluster in Desulfovibrio gigas ferredoxin II. J. Am. Chem. Soc 1986, 108 (2), 349–351.
11. Surerus KK; Munck E; Moura I; Moura JJG; LeGall J, Evidence for the formation of a ZnFe3S4 cluster in Desulfovibrio gigas ferredoxin II. J. Am. Chem. Soc 1987, 109 (12), 3805–3807.
12. Staples CR; Dhawan IK; Finnegan MG; Dwinell DA; Zhou ZH; Huang H; Verhagen MFJM; Adams MWW; Johnson MK, Electronic, magnetic, and redox properties of [MFe3S4] clusters (M = Cd, Cu, Cr) in Pyrococcus furiosus ferredoxin. Inorg. Chem 1997, 36 (25), 5740–5749. [PubMed: 11670195]
13. Honarmand Ebrahimi K; Silveira C; Todorovic S, Evidence for the synthesis of an unusual high spin (S = 7/2) [Cu–3Fe–4S] cluster in the radical-SAM enzyme RSAD2 (viperin). Chem. Commun 2018, 54 (62), 8614–8617.
14. Suess DL; Burstel I; De La Paz L; Kuchenreuther JM; Pham CC; Cramer SP; Swartz JR; Britt RD, Cysteine as a ligand platform in the biosynthesis of the FeFe hydrogenase H cluster. Proc. Natl. Acad. Sci. U. S. A 2015, 112 (37), 11455–60. [PubMed: 26324916]
15. Nicolet Y; Pagnier A; Zeppieri L; Martin L; Amara P; Fontecilla-Camps JC, Crystal structure of HydG from *Carboxydothermus hydrogenoformans*: a trifunctional [FeFe]-hydrogenase maturase. ChemBioChem 2015, 16 (3), 397–402. [PubMed: 25504963]
16. Dinis P; Suess DL; Fox SJ; Harmer JE; Driesener RC; De La Paz L; Swartz JR; Essex JW; Britt RD; Roach PL, X-ray crystallographic and EPR spectroscopic analysis of HydG, a maturase in [FeFe]-hydrogenase H-cluster assembly. Proc. Natl. Acad. Sci. U. S. A 2015, 112 (5), 1362–7. [PubMed: 25605932]
17. Rao G; Tao L; Suess DLM; Britt RD, A [4Fe-4S]-Fe(CO)(CN)-L-cysteine intermediate is the first organometallic precursor in [FeFe] hydrogenase H-cluster bioassembly. Nat. Chem 2018, 10 (5), 555–560. [PubMed: 29632334]
18. Kuchenreuther JM; Myers WK; Stich TA; George SJ; Nejatyjahromy Y; Swartz JR; Britt RD, A radical intermediate in tyrosine scission to the CO and CN^- ligands of FeFe hydrogenase. Science 2013, 342 (6157), 472–5. [PubMed: 24159045]

19. Stoll S; Schweiger A, EasySpin, a comprehensive software package for spectral simulation and analysis in EPR. J. Magn. Reson 2006, 178 (1), 42–55. [PubMed: 16188474]
20. George GN EXAFSPAK, Stanford Synchrotron Radiation Laboratory: Menlo Park, CA, 1995.
21. Binsted N; Gurman SJ; Campbell JW EXCURVE, 9.2; Daresbury Laboratory: Warrington, England, 1998.
22. Chacon KN; Blackburn NJ, Stable Cu(II) and Cu(I) Mononuclear intermediates in the assembly of the CuA center of Thermus thermophilus cytochrome oxidase. J. Am. Chem. Soc 2012, 134 (39), 16401–12. [PubMed: 22946616]
23. Chacon KN; Mealman TD; McEvoy MM; Blackburn NJ, Tracking metal ions through a Cu/Ag efflux pump assigns the functional roles of the periplasmic proteins. Proc. Natl. Acad. Sci. U S A 2014, 111, 15373–8. [PubMed: 25313055]
24. Barry AN; Blackburn NJ, A Selenocysteine variant of the human copper chaperone for superoxide dismutase. A Se-XAS probe of cluster composition at the domain 3−domain 3 dimer interface. Biochemistry 2008, 47 (17), 4916–4928. [PubMed: 18393442]
25. Suess DL; Pham CC; Burstel I; Swartz JR; Cramer SP; Britt RD, The radical SAM enzyme HydG requires cysteine and a dangler iron for generating an organometallic precursor to the [FeFe]-hydrogenase H-cluster. J. Am. Chem. Soc 2016, 138 (4), 1146–9. [PubMed: 26764535]
26. Chacón KN; Perkins J; Mathe Z; Alwan K; Ho EN; Ucisik MN; Merz KM; Blackburn NJ, Trapping intermediates in metal transfer reactions of the CusCBAF export pump of Escherichia coli. Communications Biology 2018, 1 (1), 192. [PubMed: 30456313]
27. Schrapers P; Mebs S; Goetzl S; Hennig SE; Dau H; Dobbek H; Haumann M, Axial ligation and redox changes at the cobalt ion in cobalamin bound to corrinoid iron-sulfur protein (CoFeSP) or in solution characterized by XAS and DFT. PLoS One 2016, 11 (7), e0158681. [PubMed: 27384529]
28. Barondeau DP; Kassmann CJ; Bruns CK; Tainer JA; Getzoff ED, Nickel superoxide dismutase structure and mechanism. Biochemistry 2004, 43 (25), 8038–47. [PubMed: 15209499]
29. Choudhury SB; Lee JW; Davidson G; Yim YI; Bose K; Sharma ML; Kang SO; Cabelli DE; Maroney MJ, Examination of the nickel site structure and reaction mechanism in Streptomyces seoulensis superoxide dismutase. Biochemistry 1999, 38 (12), 3744–52. [PubMed: 10090763]
30. Ryan KC; Johnson OE; Cabelli DE; Brunold TC; Maroney MJ, Nickel superoxide dismutase: structural and functional roles of Cys2 and Cys6. J. Biol. Inorg. Chem 2010, 15 (5), 795–807. [PubMed: 20333421]
31. Kuchenreuther JM; Shiigi SA; Swartz JR, Cell-free synthesis of the H-cluster: a model for the in vitro assembly of metalloprotein metal centers. Methods Mol. Biol 2014, 1122, 49–72. [PubMed: 24639253]
32. Kuchenreuther JM; Britt RD; Swartz JR, New insights into [FeFe] hydrogenase activation and maturase function. PLoS One 2012, 7 (9), e45850. [PubMed: 23049878]

Synopsis

Artificial Fe-S clusters are generated by incorporating Ni, Co or Se atoms into the 5Fe-4S cluster of the radical SAM enzyme HydG.

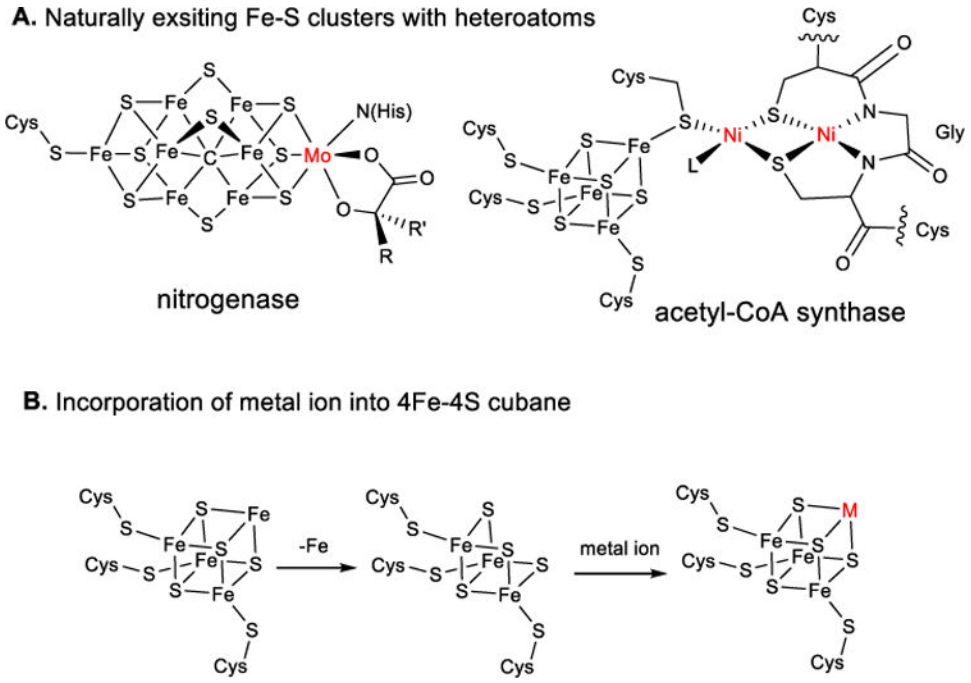

Scheme 1.

(A) Naturally existing Fe-S clusters with heterometals. (B) Established approach to incorporate metal ions into a 4Fe-4S cubane.

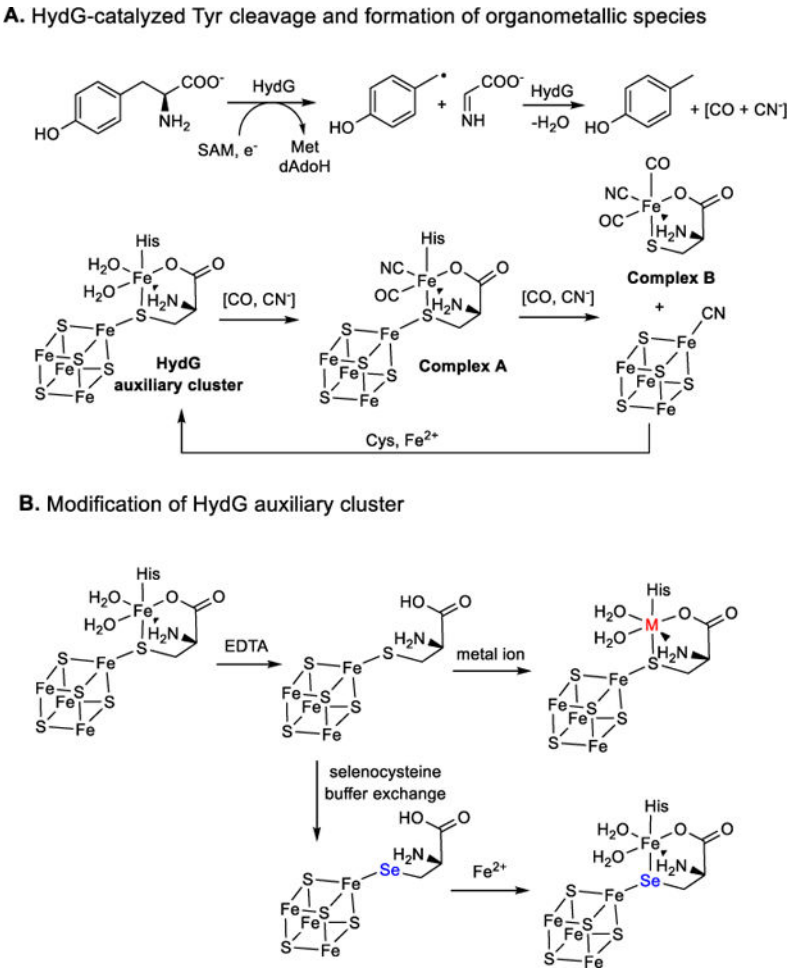

Scheme 2.

(A) HydG catalyzed reactions. (B) Incorporation of heteroatoms into the HydG auxiliary cluster in this study.

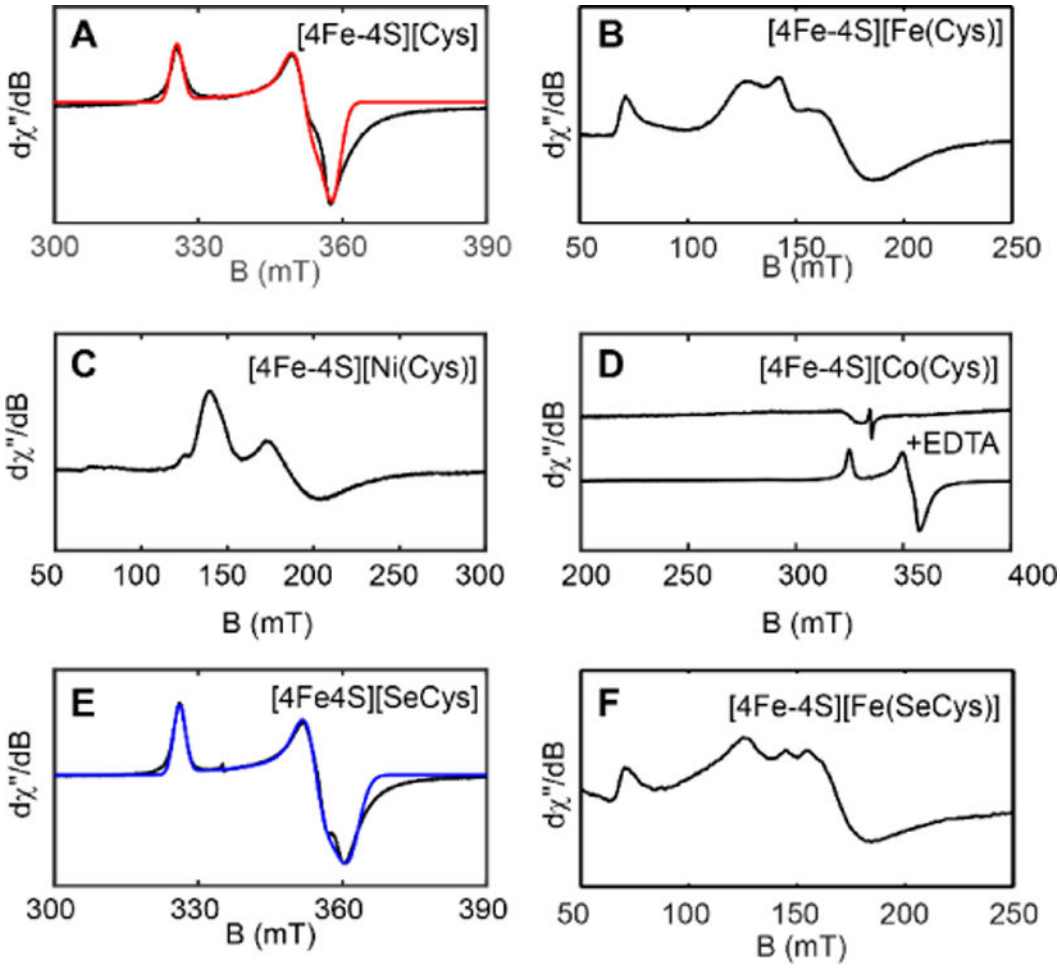

Figure 1.

X-band (9.4 GHz) EPR spectra of HydG auxiliary clusters in different forms. (A) EPR spectrum of [4Fe-4S][Cys] cluster (black trace) and simulation (red trace) with g = [2.063, 1.908, 1.876]. (B) EPR spectrum of the S = 5/2 [4Fe-4S][Fe(Cys)] cluster. (C) EPR spectrum of the S = 3/2 [4Fe-4S][Ni(Cys)] cluster. (D) EPR spectrum of the proposed [4Fe-4S][Co(Cys)] species (top trace) and the sample treated by EDTA followed by buffer exchange to remove Co(EDTA) (bottom trace). (E) EPR spectrum of the [4Fe-4S][SeCys] cluster (black trace) and simulation (blue trace) with g = [2.059, 1.895, 1.859]. (F) EPR spectrum of the S = 5/2 [4Fe-4S][Fe(SeCys)] cluster. CW EPR Conditions: temperature = 10 K, microwave power = 0.02 mW for panels A, D, and E, and 1 mW for panels B and F.

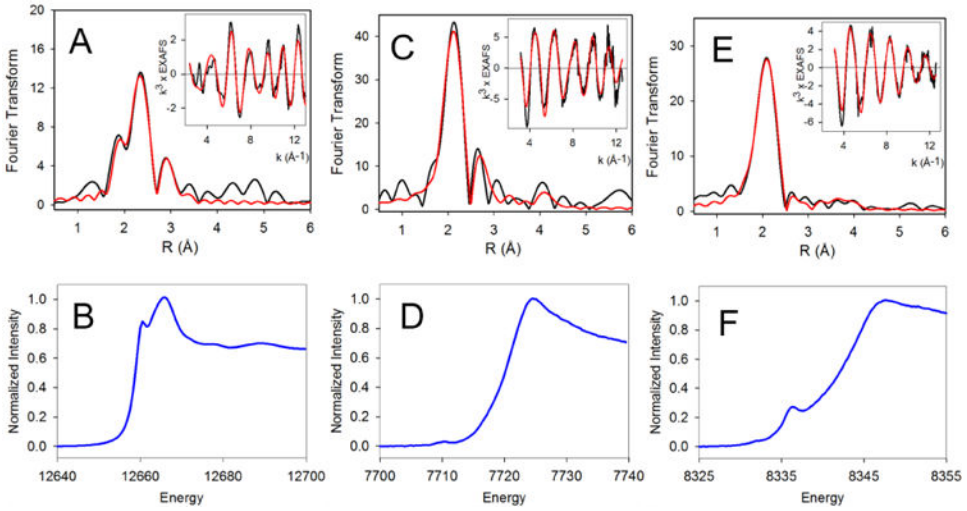

Figure 2.

Fourier transforms (top), EXAFS (top,insets), and XANES (bottom) of HydG-Se (A,B), HydG-Co (C,D), and HydG-Ni (E,F). Black traces are experimental EXAFS, red traces are simulated EXAFS, blue traces are experimental XANES. Parameters used to generate the simulations are summarized in Table 1. Transforms are phase corrected using phases associated with the nearest scatterer to each absorber, i.e. C, N, and N respectively.

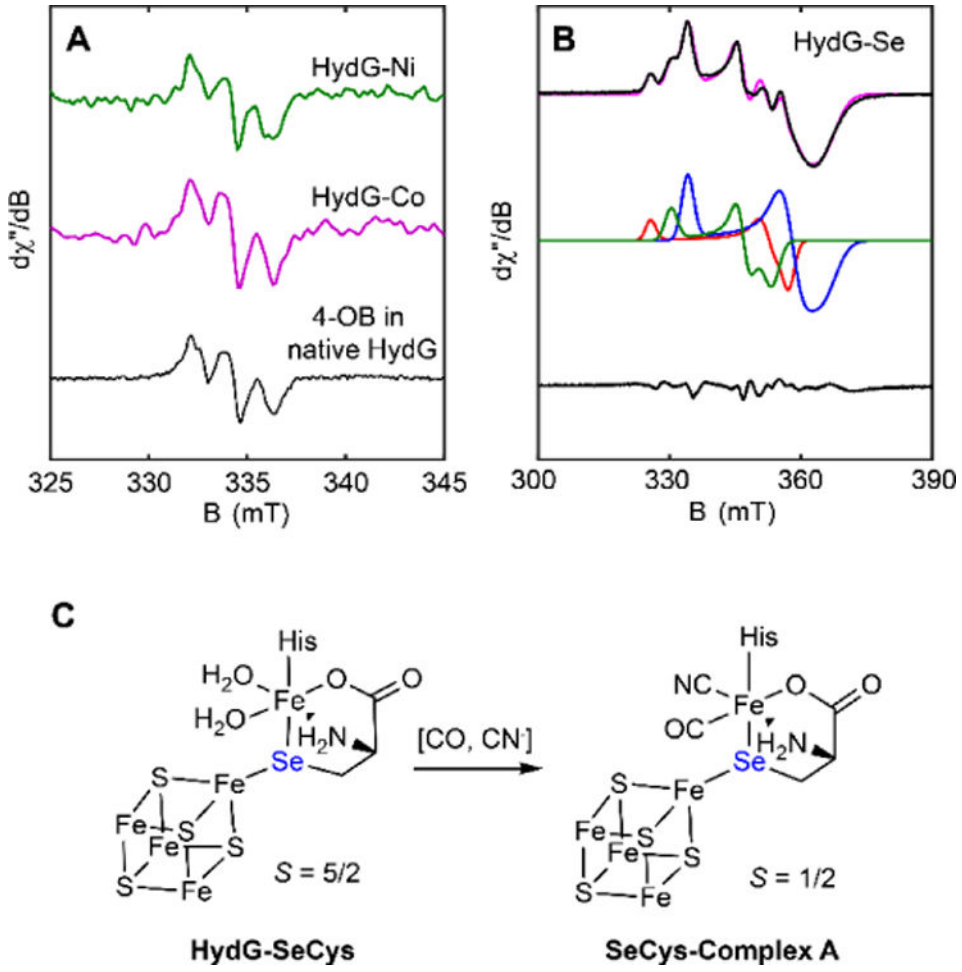

Figure 3.

Enzyme activity of HydG variants probed by EPR spectroscopy. (A) CW EPR spectra of HydG-Ni and HydG-Co reaction samples freeze-quenched at 30 s to show the formation of the 4-hydroxylbenzyl radical. Conditions: temperature = 40 K, power = 0.02 mW, modulation amplitude = 0.1 mT. (B) CW EPR spectra of HydG-Se reaction sample freeze-quenched at 30 s showing the formation of organometallic species. Top black trace: experimental spectrum. Magenta trace: total simulation. Blue trace: simulation for the SAM bound RS cluster with g = [2.0094, 1.880, 1.842], 62%. Green trace: simulation for the unknown species with g = [2.032, 1.936, 1.900], 21%. Red trace: simulation for the SeCys substituted Complex A with g = [2.062, 1.905, 1.880], 17%. Bottom black trace: difference between experimental spectrum and total simulation. Conditions: temperature = 10 K, power = 0.1 mW, modulation amplitude = 0.5 mT. (C) Scheme showing the formation of SeCys substituted Complex A.

Table 1.

Fits obtained to the Co, Ni and Se EXAFS derivatives of HydG assuming asymmetric cysteine/selenocysteine bridging between an Fe atom of the FeS cluster and the dangler Fe atom. The data support a pair of Se-Fe interactions at 2.42 and 2.62 Å respectively and a single cysteine/selenocysteine coordinated to the dangler metals as indicated in the simulated metrical parameters.

Shell	Assignment	F[a]	No[b]	R (Å)[c]	DW (Å^2)[d]	$-\Delta E_0$
Selenium						
Se-C	Cysteine –SCH_2	1.89	1	1.96(1)	0.004(2)	2.6(9)
Se-Fe[g]	FeS		1	2.418(4)	0.004(1)	
Se-Fe[g]	Dangler		1	2.619(7)	0.006(1)	
Cobalt						
Co-N	Histidine[e,f]	0.77	1	2.08(1)	0.004(1)	3.0(5)
Co-N/O	Non-His O/N[f]		4	2.08(1)	0.004(1)	
Co-S	Exogenous Cys		1	2.27(1)	0.002(1)	
Co-Fe	FeS		1	2.70(1)	0.004(0)	
Nickel						
Ni-N	Histidine[e]	0.47	1	1.926(9)	0.002(1)	1.2(5)
Ni-N/O	Non-His O/N		2	2.046(8)	0.003(1)	
Ni-S	Exogenous Cys		2	2.207(8)	0.003(1)	
Ni-Fe	FeS		Not observed			

[a] F is a least-squares fitting parameter defined as $F^2 = \frac{1}{N}\sum_{i=1}^{N} k^6 (Data - Model)^2$ where N is the number of data points and k is the photoelectron wave vector defined as $k = 2\pi/h\sqrt{(2m_e(E-E_0))}$

[b] Coordination numbers were fixed at integer values in the fits.

[c] Errors in bond lengths are reported as 95% confidence limits as determined from the least squares analysis. This underestimates the true error in the distances due to experimental factors such as finite data range, errors in the phase shifts, and choice of ΔE_0 which are strongly correlated with R. True errors are probably closer to 0.02 Å for first-shell (coordinated) ligands and 0.05 Å for outer-shell (non-coordinated) ligands.

[d] Debye Waller terms (DW) are calculated as $\exp(-2\sigma^2 k^2)$ and reported as values of σ^2 (Å^2).

[e] Fits include both single and multiple scattering contributions from the imidazole ring.

[f] In cases where the resolution ΔR for split histidine and non-histidine shells is less than the theoretical resolution of the data (π/2k), histidine and non-histidine scatterers are simulated as a single shell.